

# THE COLLAPSAR AND SUPRANOVA MODELS

CHARLES D. DERMER

*Code 7653, Naval Research Laboratory  
4555 Overlook Ave. SW, Washington, DC 20375-5352 USA  
E-mail: dermer@gamma.nrl.navy.mil*

This rapporteur review summarizes results presented in Parallel Session GBT2 (Gamma Ray Burst Theory 2) on the Collapsar and Supranova Models held 25 July 2003 at the 10th Marcel Grossmann Meeting on General Relativity, Rio de Janeiro, Brazil. A central issue in GRB studies is the process whereby energy is released from the GRB engine. One scenario is the collapsar model, where the evolved stellar core promptly collapses to a black hole surrounded by a massive, intermittently-accreting torus of nuclear density material. A second scenario is the supranova model, where the first step of a two-step collapse process leaves behind a rapidly rotating neutron star stabilized by rotation, which later collapses to a black hole while making the GRB. In the supranova model, a powerful pulsar wind lasting days to weeks after the supernova makes distinctive signatures from the heating of the supernova remnant (SNR) shell, which should be discovered with Swift. This model also predicts nonstandard reddened excesses from the cooling SNR due to the range of delays between the two collapse events, contrary to observations of SN emissions from low redshift GRBs which favor the collapsar model. The observational basis for both models is critically reviewed. Problems of the collapsar/internal shock scenario powered by the Blandford-Znajek process, and a two-collapse supranova scenario powered by the B-Z process or the Penrose mechanism, or even Ruffini's pair electromagnetic pulse, are briefly discussed. In view of the standard  $\gamma$ -ray energy upper limit, an external shock model involving jetted relativistic ejecta powered by an explosive event provides the most consistent explanation for GRB observations. An outline of a GRB model is proposed where the second collapse takes place within minutes to hours after the primary SN event, during which time loss of centrifugal support along the rotation axis of the neutron star provides a relatively baryon-clean polar environment along which a newly formed, rapidly spinning black hole drives collimated baryon-dilute outflows.

## 1 Introduction

The contributions<sup>1,2</sup> entitled “The Diagnostic Power of X-ray Emission Lines in GRBs,” by Dr. Markus Böttcher (Ohio University, USA), and “Gamma-Ray Burst Progenitors confront Observations,” by Dr. Davide Lazzati (IoA, Cambridge, UK), frame the current debate. Böttcher's article<sup>1</sup> summarizes X-ray observations, and the case is made for a supernova (SN) taking place weeks to months before the GRB, so that the circumburst medium (CBM) contains dense ( $\gtrsim 10^{10} \text{ cm}^{-3}$ ), distant ( $\approx 10^{15} - 10^{17} \text{ cm}$ ) SNR shell material whose illumination could account for the appearance of X-ray features in GRB prompt and afterglow radiation. These features give important clues about the GRB environment, and would be compelling if their significance were only greater. The marginal ( $3 - 5 \sigma$ ) detections near threshold make for concern about the reality of the features. Swift should clear this issue up, with its  $24' \times 24'$  FoV X-ray telescope reaching  $2 \times 10^{-14} \text{ ergs cm}^{-2} \text{ s}^{-1}$  in a  $10^4$  second observation, with autonomous slewing capability to get on target within one minute(!).

At the time of this writing (April, 2004), it seems probable that all GRBs have

associated SNe as identified by optically thick photospheric SN emissions appearing as reddened optical excesses in GRB afterglow light curves some 10 – 30 days after the GRB event. In low redshift GRBs, and most clearly in the case of GRB 030329<sup>3</sup>, the SN emissions are well fit by SN 1998bw light curves K-corrected and stretched to match the redshift of the GRB source. These emissions are powered by trapped shock energy and radioisotope heating (principally due to the  $^{56}\text{Ni} \rightarrow ^{56}\text{Co} \rightarrow ^{56}\text{Fe}$  decay chain formed by explosive nucleosynthesis or accretion disk winds<sup>4</sup>). The optical follow-on observations indicate that any delays between collapses to a neutron star and black hole (or strange star) last for less than a few days. This places constraints on the angular momentum and mass at formation, and the equations of state of GRB progenitors<sup>5,6</sup>.

Lazzati<sup>2</sup> argues that the issue of SN excesses in late (10 – 30 days) time optical afterglow light curves is settled, and he examines the low redshift ( $z = 0.17$ ) GRB 030329 in detail. As yet, SN excesses have not been observed from a GRB which also displays X-ray features. One possibility is that X-ray features will be detected at high significance by Swift from a GRB with a nearly coincident (within  $\lesssim$  a few days) SN, in which case the original supranova model<sup>7</sup>, with delays between the two collapse events ranging from weeks to months, is ruled out. If Fe features are firmly detected, then this might imply ejection of material from an Fe core (which then does not explain what powers the SN Ic light curve). Another possibility is that the GRBs displaying Fe features form a disjoint set from those which display SN emissions. In this case, two separate population tracks for GRBs which produce SN emissions and those which produce X-ray line features from the illumination of a distant reprocessor are implied<sup>6</sup>. It is also possible that the X-ray features are artifacts of analysis.

As is apparent, the observational situation, particularly with regard to the X-ray emission lines and absorption features and edges in GRB spectra, is murky. Then what about the theoretical situation?

The relativistic blast-wave external-shock model with both forward and reverse shock emissions is generally accepted as the basis to interpret afterglow observations, and even to apply during the prompt phase in those GRBs which display enhanced optical reverse shock radiation. At least, this model provides a serviceable tool to interpret radiation fluxes and to derive physical and environmental parameters ( $\epsilon_e$ ,  $\epsilon_B$ ,  $n_{CBM}$ , and to distinguish uniform vs. windfed CBM). The radiation processes that make  $\gamma$ -rays during the prompt ( $\approx t_{90}$ ) phase is an open question, with external and internal shock models each proposed. An external shock model, powered by a single explosive event, is favored on the basis of the data, as argued below.

In this article, supranova-model predictions of signatures of SNR shells heated by plerionic emissions emitted by a newly born, rapidly rotating and highly magnetized neutron star are presented. The heating of the SNR, and the interaction of the GRB emissions with this shell of material imply many predictions for the supranova model. We critique the collapsar and supranova models and argue that they are both inconsistent with the data (even leaving aside the X-ray observations). The observations do not (yet) show the predicted plerionic signatures of a supranova

model, nor do they imply standard reddened emissions at late times if a fraction of GRBs have delays of weeks to months between the two collapse events (that fraction, and the validity of the original supranova model, continues to decline in significance as more observations of reddened excesses accumulate). The collapsar model cannot explain the prompt GRB emissions, durations, efficiencies, nor the standard maximum-energy reservoir result. It predicts a wind-type CBM, which is only seen on rare occasion<sup>8</sup>. The baryon-dilute jet must be able to penetrate the massive stellar envelope without substantial mixing and reach  $\Gamma$  factors  $\gg 100$ .

Some new ideas are needed. One possibility is that energy is dissipated by general relativistic effects within the ergosphere of a charged, rotating black hole as it is formed, rather than extracted when a magnetized disk is accreted onto a rotating black hole, as in the collapsar model<sup>9</sup>. Numerical simulations of core collapse of massive stars show that material can be evacuated along the rotation axis of the stellar core, leaving a relatively baryon-clean environment<sup>10</sup>. Within a few minutes to 1 – 2 days of the SN, a second collapse would drive a jet in the poleward direction of the newly formed, rapidly spinning black hole to make the GRB. This model would make jet formation more feasible than in a collapsar scenario where nearly baryon-pure ejecta, whether in the form of a pair fireball or a Poynting-flux dominated flow, has to “drill a channel” through a massive stellar envelope and avoid the processes that are so effective at mixing <sup>56</sup>Co in SN 1987A, namely strong Rayleigh-Taylor mixing instabilities along the jet head and Kelvin-Helmholtz instabilities along the jet spine and in the Rayleigh-Taylor fingers.

Such a scenario does not depart from the well-established connection of long-duration GRBs with high-mass stars born in star-forming galaxies that end their lives as Type Ic SNe. Indeed, rapidly spinning Wolf-Rayet progenitor stars are the most likely GRB progenitors, as in the collapsar<sup>11</sup> and some versions (though not all<sup>12</sup>) of the supranova models. The main difference is in the nature of the collapse process and the origin and meaning of the prompt GRB emissions, with important implications for the physics of stellar evolution and black-hole formation. Whether the GRB is formed by an engine or explosion is important for understanding the physics of black hole formation. Here we argue for an explosive event (cf. Ref.<sup>[13]</sup>).

Such a model brings into focus the “standard-energy reservoir result”<sup>14</sup> or, more accurately, the “standard-energy upper limit”<sup>15</sup>, and avoids many unpleasant issues that are often avoided in discussions of the collapsar scenario, such as low efficiency and absence of curvature signatures that are expected from colliding shells in the internal/external scenario, and the frequent presence of a rather uniform CBM as inferred from afterglow model fits to the external shock emissions<sup>16</sup>. I also comment on current models for energy extraction from a rotating black hole, including the Blandford-Znajek effect and the Penrose mechanism.

Both the collapsar and supranova models have difficulties to explain the GRB phenomenon. We<sup>17,18</sup> have argued that the pulses in a GRB light curve are flashes made when a relativistic blast wave intercepts density inhomogeneities in the CBM. Delayed low-level radiations from fallback onto the newly formed black hole are possible (and this could help explain X-ray features should they turn out to be real). The GRB light curves are compatible with an explosion or a magnetar

discharge<sup>19</sup>. The relativistic ejecta shell can support a reverse shock structure to explain prompt optical and early radio afterglows.

Reviews of GRB physics and observations that focus on observations<sup>20</sup> and theory<sup>21</sup>, both from the perspective of the external shock model<sup>22</sup> and the internal/external scenario<sup>23,24</sup>, can be consulted for further background.

## 2 The GRB/Supernova Connection

The discovery that the GRBs which are observed today took place at cosmological distances led to the development of the relativistic fireball/blast-wave model<sup>21</sup> that generalizes the theory of SNe to cosmic explosions with relativistic ejections. The coasting Lorentz factors  $\Gamma$  of GRB outflows reach values of  $10^2 - 10^3$ , as quantified by  $\gamma\gamma$  attenuation calculations<sup>25,26,27</sup>. Associated with this discovery are other important observational results<sup>20</sup> that tie the long-duration ( $t_{90} \gtrsim 1$  s) GRBs to high mass stars and thence to SNe or some subset of SNe:

- GRB host galaxies have blue colors, consistent with galaxy types that are undergoing active star formation<sup>28,29</sup>.
- GRB counterparts are found within the optical radii and central regions of the host galaxies, consistent with locations within star-forming spiral arms<sup>30</sup>.
- In some cases (e.g., GRB 011121), the surrounding medium is better fit with a wind-fed than uniform CBM<sup>8</sup>;
- Lack of optical counterparts in some GRBs may be due to high column densities and extreme reddening from large quantities of gas and dust in the host galaxy<sup>31</sup>, as found in molecular cloud complexes where massive stars are born.
- In other cases, however, the *HETE-2* mission has shown that the “dark optical GRBs” are due to the large range of temporal indices of GRB optical light curves, which are sometimes very steep and rapidly fading<sup>32</sup>.
- GRBs are associated with nearly contemporaneous Type Ic SNe in low-redshift bursts where detection of the SN emissions are possible (see Section 4);
- GRB outflows are in the form of highly collimated jets. The evidence for beaming is inferred from achromatic beaming breaks in optical afterglow light curves that occur when the Doppler cone of the decelerating relativistic outflow is about the same size as the opening-angle of the jet<sup>33</sup>.

From the beaming breaks, Frail et al.<sup>14</sup> inferred that the mean solid angle subtended by *observed* GRB jets is about 1/500th of the full sky, so that the mean beaming factor  $f_b = 0.2\%$ . As a consequence, there are many hundreds of GRBs events that take place for every one that is detected. The absolute total energies in  $\gamma$ -rays from most GRBs cluster within a factor of  $\approx 2$  of  $\sim 1.3 \times 10^{51}$  ergs<sup>15</sup>, typical of the kinetic energy in SN ejecta. By performing the statistics of GRB

sources, one<sup>34</sup> finds that the rate of GRBs in the Milky Way could reach  $\approx 10\%$  of the rate of Type Ib/c SNe.

The value of  $f_b$  is currently a subject of debate and is in any case not precisely defined for structured jets. Larger values of  $f_b \approx 0.01 - 0.1$  are sometimes claimed, which makes the individual GRB event rarer and more energetic, even if the local time- and space-averaged power into a star-forming galaxy remains about the same based on the hard X-ray/ $\gamma$ -ray output,  $\approx 10^{44}$  ergs Mpc<sup>-3</sup> yr<sup>-1</sup>. Thus, not all Type Ic SNe harbor a GRB, and the fraction of Type Ic SNe that host GRB explosions may be as small as 1%. Nearby GRBs are likely to radiate less energy in  $\gamma$ -rays relative to ejecta kinetic energy compared to more distant GRBs<sup>13</sup>. Rapidly fading GRBs also tend to be underluminous in  $\gamma$ -ray energy<sup>15</sup>.

These lines of evidence suggest that GRBs are produced by collimated relativistic plasma ejected during an explosion or an active engine phase of a subset of Type Ic SNe formed from the collapse of the cores of high-mass stars.

### 3 X-Ray Features and the Supranova Model

This section critiques M. Böttcher's contribution<sup>1</sup>. See his article for more details, including additional references to the original literature.

X-ray features have now been detected in at least 8 GRBs. Table 1 of Ref. [1] summarizes these observations, but the most important results are:

1. low significance X-ray Fe K feature observed from GRB 970508<sup>35</sup> in a secondary outburst with Beppo-SAX, consistent with an <sup>56</sup>Fe Ly $\alpha$  emission line blue-shifted by 0.1c from the redshift ( $z = 0.835$ ) of the GRB source;
2. low significance X-ray Fe K feature observed in GRB 970828<sup>36</sup> ( $z = 0.958$ ) with ASCA, which is only consistent with the redshift of the GRB host galaxy if the feature is identified with an Fe K recombination edge in a nonequilibrium situation;
3. X-ray emission features observed in the afterglow spectra of GRB 991216 ( $z = 1.00$ ) with Chandra<sup>37</sup>, identified with H-like Fe and a recombination edge of Fe, along with weaker evidence for a recombination edge and emission line of H-like S, which originate in an outflowing moving at  $\sim 0.1c$  with respect to the source redshift;
4. variable and declining Fe absorption lasting for the first  $\approx 14$  s of the  $\gamma$ -ray luminous phase of GRB 990705<sup>38</sup> at  $z = 0.8435$ ;
5. an X-ray feature observed from GRB 000214<sup>39</sup> with Beppo-SAX, which had no optical transient counterpart or redshift measurement, but if identified with Fe K $\alpha$ , corresponds to  $z = 0.47$ ;
6. multiple high-ionization emission features of S XVI, Si XIV, Ar XVIII and Ca XX (but no Fe K $\alpha$  emission line or edge) observed from GRB 011211<sup>40</sup> ( $z = 2.14$ ) with XMM-Newton (whose reality has been questioned);

7. low significance high-ionization Si XIV and S XVI blueshifted by  $0.12c$  with respect to the host galaxy redshift ( $z = 1.254$ ) observed from GRB 020813<sup>41</sup> with XMM-Newton from a GRB triggered by HETE-II; and
8. low significance high-ionization S and Si (no Ni or Fe) emission features observed with XMM-Newton from GRB 030227 triggered by the INTEGRAL Burst Alert System<sup>42</sup>. The emission lines appeared in one segment of the observation, and the X-ray spectrum was lineless in an earlier segment. The redshift was not measured directly, but equal to  $z = 1.32$  and  $1.34$  for Si XIV and S XVI, respectively, which when transformed from the emission to the observer frame implies  $z \approx 1.6$ .

These results, taken individually and as a group, indicate that GRBs take place in environments highly enriched in metals, such as active star-forming regions. A highly metal-enriched and dense shell of material surrounds the sources of GRBs, and this shell is sometimes moving at speeds of  $\approx 0.1c$  with respect to the source. A major concern is that although the significance is rather marginal, the amount of line energy is uncomfortably large and approximately constant, ranging from about  $6 \times 10^{48}$  ergs per line in GRB 030227 to  $\approx 2 \times 10^{49}$  ergs for GRB 970508. The line fluorescence is typically detected over observing time scales of  $\approx 10^4$  s. The line energies in the sample of GRBs have tended to drop by a factor  $\approx 4$  in the later bursts, but this trend may be misleading. Another oddity is that although  $^{56}\text{Fe}$   $K\alpha$  emission was reportedly observed in the first four GRBs, only emission lines associated with Si, S, Mg, and Ca were seen in the later GRBs when XMM-Newton was used, which may however reflect the different capabilities of the respective X-ray telescopes.

Taking the observations at face value leads to some immediate requirements for models.

If the total  $^{56}\text{Fe}$   $K\alpha$  line energy is  $10^{49} E_{49}$  ergs, then the number of Solar masses in  $^{56}\text{Fe}$  if each ion is individually illuminated once is

$$\frac{M(^{56}\text{Fe})}{M_{\odot}} = \frac{10^{49} E_{49} \text{ ergs}}{5F_5(1 M_{\odot}/56m_p) \cdot 13.6(26^2)Z_{26}^2 \text{ eV}} \cong \frac{6E_{49}}{F_5 Z_{26}^2}, \quad (1)$$

where  $F = 5F_5$  is the fluorescence yield. That's a lot of Iron, which if made through stellar explosive nucleosynthesis, must already have decayed ( $^{56}\text{Ni}$  decays through electron capture<sup>43,44</sup>, so the decay timescale could even be longer than  $\approx 100$  days).

Type II SNe are thought to release perhaps  $\approx 0.07M_{\odot}$  of  $^{56}\text{Ni}$ , and Type Ia as much as a Solar mass. Even if Type Ic SNe release  $\approx 0.5M_{\odot}$  of  $^{56}\text{Ni}$ , multiple ionization episodes from a dense medium are required to account for the extraordinary energy and equivalent widths of the emission lines and absorption features.

Another constraint<sup>45,46</sup> applies to the size scale of the emitting region, which is assumed to be moving at most at mildly relativistic speeds. From the duration  $t_{line}$  of the line observations, given in units of  $10^4 t_4$  s, then

$$(1 - \cos \theta_{shell})R \lesssim \frac{ct_{line}}{1+z} \cong \frac{3 \times 10^{14} t_4}{1+z} \text{ cm}, \quad (2)$$

where  $\theta_{shell}$  is the angle between the fluorescing or absorbing shell medium and the observer. If the target material is moving in the transverse (equatorial) direction at the speed of  $0.1v_{-1}c$ , a *torus* geometry is natural. This implies that the maximum duration between a first and second collapse event is  $\lesssim v_{-1}^{-1}$  day, assuming that the ionizing radiations travel near light speed. Vietri et al.<sup>45</sup> and Böttcher<sup>47</sup> and Fryer<sup>48</sup> consider a model where an expanding shell materially impacts and shocks a torus of material. This geometry permits only short time delays between the shell ejection and the GRB and X-ray line production. The target shell material could be from an intense progenitor wind formed during the common envelope phase of a compact object and helium star.

A *distant reprocessor* could be  $\approx 10^{15} - 10^{17}$  cm away and contain clumps of highly enriched material with densities  $\gtrsim 10^{10}$  cm<sup>-3</sup>. Variable X-ray absorption is essentially undetectable from a GRB surrounded by a uniform CBM, even if highly enriched<sup>49</sup>. Extremely clumped ejecta<sup>50</sup> or blueshifted resonance scattering in a high-velocity outflow<sup>46</sup> can account for the variable absorption in GRB 990705. In this geometry, a shell of material is illuminated by the GRB emissions and could originate from a SN taking place months earlier. The target material would have locations and size scales corresponding to requirements of the external shock model for the prompt phase<sup>17</sup>. There are ranges of ionization parameters that are compatible with the observations for a geometry-dominated model, though not an engine-dominated (i.e., collapsar) model<sup>51</sup>.

Considerable heating accompanies multiple recombinations and reionizations, thereby reducing the recombination rate coefficient, so this model is criticized to make such a large line energy. Pair production could enhance the line production efficiency. Other possibilities includes a funnel geometry<sup>52</sup> with a long-lived photoionizing source, which has not been detected<sup>53</sup>, and a pair screen<sup>54</sup> to provide a local flux of UV/X radiation. The question of whether photoionization models or thermal models (or both) apply remains an open question.

Taken together, the earlier ejection of a stellar envelope would be advantageous to explain the X-ray features, as in the supranova model<sup>7</sup>. This reasoning, given also the results in Chapter 2, leads to the conclusion that GRBs are a subset of SNe powered by a two-step collapse to a black hole of a massive ( $\gtrsim$  several  $M_{\odot}$ ) core stripped of its H and He envelope. The collapse event drives a subrelativistic outflow to power the SN, and a relativistic outflow to power the GRB. The GRB outflow is likely to be highly collimated. The excitation of torus material or the illumination of shell material in the polar direction could produce the line signatures. Possible stellar progenitor candidates are Wolf-Rayet stars<sup>11</sup>, or merger events involving He cores<sup>55,50</sup>.

If the X-ray identifications of Fe features are real, then GRB SNe must yield  $\sim 1M_{\odot}$  of <sup>56</sup>Fe, which is a challenge for any model.

#### 4 Delayed Reddened Excesses and SN Light Curves

This section critiques and updates D. Lazzati's contribution<sup>2</sup>, and summarizes evidence for SN emissions in the light curves of GRBs and implications for GRB

source models based on the examples of GRBs 980425 and 030329.

GRB 980425, discovered with Beppo-SAX, was a smooth-profiled GRB with mean duration  $\sim 20$  s, and is likely associated spatially and temporally with the Type Ic SN 1998bw in a spiral host galaxy at a distance of  $\approx 40$  Mpc. Its apparent isotropic  $\gamma$ -ray energy was only  $\approx 10^{48}$  ergs. It displayed very intense radio emissions, indicative of a related mildly relativistic outflow. GRB 980425 was probably an off-axis event with a much lower  $\gamma$ -ray to kinetic luminosity than in other GRBs. The kinetic energy is estimated from the radio luminosity using minimum energy arguments, or by multiplying the X-ray luminosity with time at a fixed observing time (e.g., 8 hours after the GRB) when the electrons are in the fast cooling regime and making a correction factor for the number of ions per electron<sup>58</sup>. The kinetic energy inferred from the radio luminosity of SN 1998bw was  $\gtrsim 10^{49}$  ergs<sup>59</sup>, and exceeds  $10^{52}$  ergs when modeling the SN light curve<sup>60</sup>. These energies are similar to the kinetic energy of the Type Ic SN 2003L, but orders of magnitude greater than the radio luminosity in the Type Ic SN 2002ap.

Comparison of GRB 980425 with the low redshift ( $z = 0.17$ ) GRB 030329 associated with SN 2003dh is instructive. Based on the jet-break times, typical beaming-corrected GRB energies have a “standard”  $\gamma$ -ray energy reservoir of  $\sim 10^{51}$  ergs<sup>14,15</sup> (see Section 5). GRB 030329 displayed an early optical jet break at  $\approx 0.4$  d, and a much later 15 GHz jet break at  $\approx 15$  d. In contrast, GRB 030329 has a  $\gamma$ -ray energy  $E_\gamma \approx 2 \times 10^{50}$  ergs<sup>61</sup>, and is therefore underenergetic compared to a “typical” GRB (as also are XRF 020903 and GRB 980425). But in each of these cases, the kinetic energies  $E_{ke} \gtrsim 10^{51}$  ergs<sup>62</sup>. (By contrast, GRB 031203, at  $z \cong 0.1$ , which is very similar to GRB 980425, has  $E_\gamma \approx 10^{50}$  ergs and  $E_{ke} \approx 2 \times 10^{49}$  ergs.)

All this evidence points to a highly structured jet, or a “spine in sheath” geometry (as in the case of 3C 273<sup>63</sup>) to account for GRB detectability and phenomenology. A dirty/clean standard top-hat jet fireball model is too simplified. Even if one wished to maintain a unifying approach to GRB observations, then angle-dependent effects from a structured jet must be considered. In any case, the number of GRBs hosted by Type Ib/c SNe should be  $\lesssim 10\%$ .

The discovery that a SN emerges in the afterglow of GRB 030329 tells us that at least a fraction of SNe host GRBs, and that SN and GRB explosions are most likely simultaneous<sup>2</sup> or, at most, separated by a few days. Here summarizes the evidence for delayed reddened excesses from SN emissions in GRB optical afterglows:

1. GRB 970228 at  $z = 0.695$ , which reached a flux at  $\nu = 3.8 \times 10^{14}$  Hz at  $\approx 38$  d after the GRB<sup>64,65</sup> of  $F_\nu \cong 0.87 \mu\text{Jy}$ , corresponding to a stationary-frame luminosity of  $4\pi d_L^2 \nu F_\nu(t = 25 \text{ d}) \cong 10^{43}$  ergs  $\text{s}^{-1}$  ( $d_L = 1.4 \times 10^{28}$  cm), about the same as the SN 1998bw template. Reichart<sup>64</sup> argues that this emission signature cannot be explained with a dust echo.
2. GRB 980326 with unknown redshift<sup>66</sup>. The peak of the light curve at 6558 Å (R-band is 7000 Å, 1.8 eV,  $\nu = 4.3 \times 10^{14}$  Hz) appears at  $\sim 20$  days and has a peak flux density  $\approx 0.4 \mu\text{Jy}$ , or a  $\nu L_\nu$  power of  $\approx 10^{43}$  ergs  $\text{s}^{-1}$  if  $z \sim 1$ .
3. GRB 980425 ( $z = 0.0085$ , or  $d \approx 40$  Mpc) associated with the Type Ic SN



1998bw<sup>67,68</sup>. With a peak absolute luminosity  $\approx 1.6 \times 10^{43}$  ergs s<sup>-1</sup>, it requires  $\sim 0.7 M_{\odot}$  of <sup>56</sup>Ni to power the light curve<sup>60</sup>.

4. GRB 980703 at  $z = 0.9661$ , consistent with a SN 1998bw-type excess at  $\approx 10 - 20$  days after the GRB, or no SN<sup>69</sup>.
5. GRB 000418 at  $z = 1.119$ , which had R-band emission exceeding  $\approx 1 \mu\text{Jy}$  40 days after the GRB. If due to jetted afterglow emission, this flux would correspond to a  $\nu L_{\nu}$  luminosity  $\approx 3 \times 10^{43}$  ergs s<sup>-1</sup> that could conceal a SN excess<sup>70</sup>.
6. GRB 000911 with a host galaxy redshift of  $z = 1.06$  and optical emission with luminosity  $L \sim 1.5 \times 10^{43}$  ergs s<sup>-1</sup> after  $\approx 1$  week. The addition of a SN 1998bw-type excess improves the fit, and an alternative model of a shock interacting with WR progenitors involves several free parameters<sup>71</sup>.
7. GRB 011121 at  $z = 0.362$  with a distinct reddened excess appearing at  $\approx 20$  days after the GRB and reaching a  $\nu L_{\nu}$  power of  $\approx 2 \times 10^{42}$  ergs s<sup>-1</sup> at 7020Å. This delayed emission is well fit by a SN1998bw template emission, and the agreement improves if GRB 011121 exploded  $\sim 3 - 5$  days after the SN<sup>72,8</sup>.
8. GRB 010921 at  $z = 0.451$ , which showed no SN to a limit 1.33 magnitudes fainter than SN 1998bw at the 99.7% confidence limit<sup>73</sup>.
9. GRB 020405 at  $z = 0.690$ , which showed a delayed reddened excess consistent with a SN 1998bw emissions dimmed by 0.5 magnitude<sup>74,75</sup>. The radio data are not consistent with a density profile  $\propto r^{-2}$ .
10. GRB 020410, redshift unknown, that exhibited an optical rebrightening one week after the GRB consistent with SN emissions from a nearly coincident SN<sup>76,77</sup>.
11. GRB 030329, associated with SN 2003dh at  $z = 0.1685$ , with a highly variable optical component<sup>78,79,3</sup>.
12. The X-ray flash XRF 031203 at  $z = 0.1055$ , associated with SN 2003lw, which can be represented by SN1998bw brightened by 0.55 mag<sup>80</sup>.

These observations show that in many cases, GRBs and XRFs are accompanied by a nearly contemporaneous SN which is spectrally much like the Type Ib/c SN 1998bw that is temporally and spatially associated with GRB 980425.

A collapsar model GRB must have a progenitor with stellar photospheric radius  $\lesssim 10^{11}$  cm, which limits allowed progenitors to massive stars that have lost their H and He envelopes, such as Wolf-Rayet stars or close binary systems<sup>81</sup>. They must keep the ejecta extremely baryon-free by pushing away  $\sim 0.01 M_{\odot}$  while retaining a baryon purity  $\lesssim 10^{-3} M_{\odot}$  mixed in with the explosion. A model for jet emission must explain the Amati relation<sup>82</sup>, where the  $\nu F_{\nu}$  peak energy  $E_{pk} \propto E_{iso,\gamma}^{1/2}$ , where  $E_{iso,\gamma}$  is the apparent isotropic energy release.

Although Lazzati had argued that the bumps and wiggles in the light curve of GRB 021004<sup>83</sup> were due to density enhancements in the CBM, he abandons that model for a model with episodes of delayed injection to explain the complex optical light curve of GRB 030329<sup>79</sup>. He claims that ‘any event that takes place over the entire fireball surface’ will produce deviations in the afterglow light curve ‘on timescales  $\delta t \sim T$ , where  $T$  is the moment in which the deviation begins.’ ” This argument does not apply when the size scale of the density irregularities is much smaller than  $\Gamma^{-1}$ , which is the most interesting regime from the point of view of an external shock model. Besides the complexity expected in the CBM<sup>84</sup>, special relativistic effects<sup>17,18</sup> enhance emissions from shell-cloud interactions for clouds with  $\theta \ll 1/\Gamma$ .

The problem of the interpretation of the optical polarization curve of GRB 030329 may be solved if complex behavior in its optical afterglow light curve is a result of localized blast-wave/cloud interactions in an external shock model.

## 5 The Standard Energy Reservoir and the Collapsar Model

Because of the potential importance of this finding, the “standard energy reservoir” result is summarized before enumerating the internal contradictions of the collapsar model.

The standard  $\gamma$ -ray energy release from a GRB holds at least as an upper limit within a factor of  $\approx 2$ , and was originally quoted as  $E_\gamma \approx 3 \times 10^{51}/(\eta_\gamma/0.2)$  ergs<sup>14</sup>, with the efficiency for  $\gamma$ -ray production compared to the total energy in the outflow given by  $\eta_\gamma \approx 0.2$ . The absolute  $\gamma$ -ray energy from a GRB is given by  $E_\gamma = f_b E_{iso,\gamma}$ , where the beaming factor  $f_b = 1 - \cos \theta_j$ ,  $E_{iso,\gamma} = 4\pi d_L^2 F_\gamma/(1+z)$ , and the jet-opening half-angle given by<sup>14</sup>

$$\theta_j = 0.057 \left( \frac{t_j}{1 \text{ day}} \right)^{3/8} \left( \frac{1+z}{2} \right)^{-3/8} \left[ \frac{E_{iso,\gamma}}{10^{53} \text{ ergs}} \right]^{-1/8} \left( \frac{\eta_\gamma}{0.2} \right)^{1/8} \left( \frac{n}{0.1 \text{ cm}^{-3}} \right)^{1/8}. \quad (3)$$

Note the weak dependencies on the unknown densities and efficiencies, which can be further constrained by afterglow modeling and comparison of the measured  $\gamma$ -ray energy with the kinetic energy of the flow.

The standard  $\gamma$ -ray energy reservoir result is now superseded by observations<sup>15</sup> of low  $E_\gamma$  outliers GRBs 980425, 030329, and 031203 which are underluminous, implying that the standard  $\gamma$ -ray energy is an upper limit and that there are biases favoring the detection of distant GRBs with maximum energy release.

This result is quite difficult to explain in the context of a collapsar scenario, where the relativistic jet passes through a massive dense stellar envelope. A “large diversity in any accompanying SN components of GRBs is expected,” and only a tiny fraction of a Solar mass of baryons mixed into the explosion would make for a considerably different amount of energy in  $\gamma$ -rays, so the “apparent constancy of the gamma-ray energy release is even more mysterious<sup>72</sup>.”

Some other particulars which an internal shock/collapsar model must answer to be viable are:

1. How is it possible for pulses in GRB blast waves to have high efficiency in an internal shock model and also to have approximately constant (within a factor of 2 – 3) values of peak photon energy  $E_{pk}$  in different pulses of the same GRB in spectra that extend to hundreds of MeV?
2. If internal shells have such widely different efficiencies, then how is the standard  $\gamma$ -ray energy reservoir result explained?
3. Why are curvature effects from spherical GRB blast waves, as found in an internal shock scenario, rarely if ever seen in GRB pulse profiles<sup>85,86</sup>?
4. How is it possible for a jet to pass through a massive stellar envelope of several light seconds width and create pulses that are fractions of a second long?
5. If the collapsar model is a failed SN, that is, there is no associated SN, then how is the enormous amount of  $^{56}\text{Ni}$  produced to power the light curve<sup>9</sup>?
6. Why have there been no detailed comparisons between temporal and spectral characteristics of GRB pulses, or even a smooth fast-rise, slow decay light curve, to show whether an internal shock scenario with high efficiency can explain GRB data?

An external shock model with a single relativistic blast wave can simply answer these questions:

1. An external shock model is much more efficient than an internal shock model<sup>18</sup>, and approaches 100% efficiency for  $\gamma$ -ray production from accelerated electrons when the CBM is sufficiently dense. The values of  $E_{pk}$  are relatively constant because the relative Lorentz factor in the interactions is about the same for interactions within the Doppler beaming cone.
2. The most energetic GRBs are those where the largest fraction of the available kinetic energy is dissipated in the form of  $\gamma$  rays.
3. Curvature effects are not expected to be seen in an external shock model where the blast wave intercepts inhomogeneities on angular scales smaller than  $\approx 1/\Gamma$ .
4. The jet originates from a bare collapse into a medium that has already been evacuated of much of the dense material.
5. A two-step collapse process would first form a SN with a large amount of  $^{56}\text{Ni}$  production, and would later collapse to a black hole to produce the GRB.
6. Comparisons of pulse profiles, time histories, and phenomenology with an external shock model are favorable<sup>87,88</sup>.

Zhang and Mészáros<sup>21</sup> review the debate.

## 6 The Heated SNR Shell in the Supranova Model

Any viable GRB model must be able to explain the increasing evidence for supernova-like emissions in the optical afterglows within the context of a model that explains the highly variable pulses in the prompt phase of a GRB. The evidence for X-ray features in prompt and afterglow GRB spectra indicates that high density, high metallicity material near GRB sources.

Is it possible to construct a model to explain at the same time the X-ray features and the delayed reddened excess emissions? Could a SNR shell that is illuminated and heated by a pulsar wind (PW) and cools following the GRB event make emissions that explains the delayed reddened excesses seen from GRBs?

We<sup>89</sup> have tried to construct a model within the context of the two-step collapse process in the supranova scenario. This model has a number of attractive features: the period of activity of a highly magnetized neutron star preceding its collapse to a black hole can produce a pulsar wind bubble consisting of low density, highly magnetized pairs<sup>56,57</sup>, in accord with afterglow model fits<sup>16</sup>. The heating of the SNR shell by the X-ray synchrotron radiation from the pulsar wind electrons could provide an important source of ionizing radiation. A cooling SNR shell could produce the excess reddened emissions.

We have found, however, that such a solution for the reddened excesses requires fine-tuning and, if not fine-tuned, predicts a wide range of cooling emissions that have not yet been observed. (It is important, however, to measure the spectra of SN emissions from nearby GRBs to determine how similar they are to SN 1998bw.) Thus the original supranova scenario appears not to be compatible with observations of SN emissions if all GRBs, as seems probable, display rather uniform SN emissions in GRB optical afterglows.

If the delayed reddened excesses in GRBs cannot be explained by the supranova model, it is ruled out. A simple derivation of the emissions from a SNR shell heated by a PW is presented in the Appendix.

The results of that analysis are displayed in Fig. 1, which shows the total  $\nu L_\nu$  flux composed of synchrotron, SSC, and thermal components. Standard parameters are used, as defined in the Appendix. The heavy solid and dashed curves correspond to standard parameters with  $t/t_{sd} = 0.1$  and  $0.01$  as labeled, where  $t_{sd}$  is the magnetic dipole spin-down timescale, the crossing (or dynamical) timescale of the shell  $t_{dyn} = 32.4$  and  $3.2$  days, and  $T_{eff} = 1700$  and  $5420$  K, respectively ( $t_{sd} = 3240$  d). This system is in accord with the standard supranova model and might explain the delayed excess emission in GRB 011121, but requires fine-tuning. The set of three dotted curves employ standard parameters, except that  $B_{12} = 4$ , and  $t/t_{sd} = 1, 0.1$ , and  $0.01$  as labeled ( $t_{sd} = 202$  d), with  $t_{dyn} = 20.2, 2.0$ , and  $0.2$  days ( $= 17$  ks), and  $T_{eff} = 3760, 11900$ , and  $37630$  K, respectively.

The intense PW X-ray synchrotron emission provides a source of ionizing photons throughout the SNR shell that would decay on the timescale  $t_{dyn}$  (the line flux would decay on  $\approx 2t_{dyn}$  due to emissions from the far side of the shell). The  $B_{12} = 4, t/t_{sd} = 0.01$  case might correspond to a GRB 011211-type system. The PW radiation field provides an additional source of ionizing photons in the supranova model, and would be energetically important for this case if the typical en-

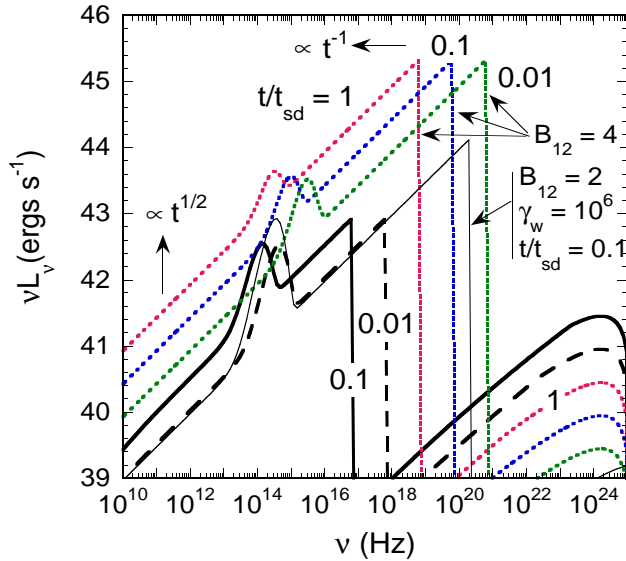


Figure 1. Total model spectral energy distribution composed of synchrotron, synchrotron self-Compton, and shell thermal emission from a pulsar wind and wind-heated SN shell. Standard parameters, given in the Appendix, are used, except where noted in the legends.

ergies of electrons injected by the pulsar wind is  $\gamma \cong 10^4$ . A varying ionization flux impinging on an expanding SNR shell will produce a characteristic kinematic signature of shell illumination.

The thin solid curve is the result for standard parameters except that  $B_{12} = 2$ ,  $\gamma_w = 10^6$ , and  $t = 0.1t_{sd} = 81$  d. For this case,  $t_{dyn} = 8.1$  d and  $T_{eff} = 4360$  K. It is apparent that a range of parameter could make quasi-thermal emission between  $\sim 10^{14} - 10^{15}$  Hz at the level of  $\sim 10^{42} - 10^{43}$  ergs  $s^{-1}$  some tens of days after the GRB event, but only if accompanied by intense heating from the plerionic synchrotron radiation.

Thus, a delayed reddened excess from the cooling shell may be seen, for plausible parameters, some tens of days after the GRB even if the GRB takes place months after the SN. The PW heating is in addition to any heating due to the Ni  $\rightarrow$  Co  $\rightarrow$  Fe chain, and may relax the need to have  $\gtrsim 0.5M_\odot$  of  $^{56}Ni$ , as required to explain the unusually bright light curve of SN 1998bw<sup>60</sup>. Whether the heated shell looks like the observations of reddened emissions in the optical emissions of GRBs will require better observations of Type Ic SNe and low-redshift GRBs, and better studies of this system.

Should this model be correct, then GRBs would exhibit a bright hard X-ray emission feature corresponding to the plerionic component that could be detected with INTEGRAL or Swift from nearby  $z \lesssim 0.1 - 0.3$  GRBs when the PW synchrotron flux radiates  $\gtrsim 10^{44}$  ergs  $s^{-1}$  at X-ray energies. A nonthermal optical emission signature would accompany the reddened excess, with a relative intensity that depends sensitively on the energies of the PW electrons accelerated. A hard X-ray sky survey instrument such as EXIST could monitor for the PW nonthermal emission preceding aligned and off-axis GRBs. The X-ray synchrotron radiation

provides a source of external radiation to enhance photomeson production by energetic hadrons over the standard GRB model<sup>95</sup>.

The supranova model makes a number of other predictions:

1. Compton-scattered  $\gamma$  radiation from GRB electrons scattering photons from the intense plerionic radiation field<sup>57,94</sup>;
2. High-energy neutrinos from the interactions of accelerated protons with the SNR shell, and due to photomeson production with the external radiation field<sup>95,96,97</sup>.
3.  $\gamma$ -ray emissions from the newly-formed, rapidly rotating pulsar<sup>6</sup> prior to the second collapse to a black hole.

## 7 Energy Release from a Newly Formed, Rapidly Rotating Black Hole

At the heart of the GRB debate is the process that liberates an enormous amount of energy over a very short time in the form of a collimated plasma outflow with very small baryon contamination. Though some models have considered highly magnetized pulsar emissions<sup>19</sup> or (as was discussed in the Session) collapse to quark matter<sup>98</sup>, it is generally assumed that GRBs are powered by the birth of a newly formed black hole. Until the question of the power source of GRBs is solved, problems about the origin of <sup>56</sup>Ni, which is supposed to power the reddened excesses observed in Type Ic SNe—whether from explosive nucleosynthesis or disk winds<sup>4</sup>—cannot be solved.

Here we assume that a GRB is powered by the birth of a newly formed, rapidly spinning black hole. In addition to the enormous gravitational energy available during the collapse process, a spinning black hole can be formed with  $\gg 10^{52}$  ergs of rotational energy. Ruffini and colleagues<sup>99</sup> argue that polarization of the vacuum can produce an  $e^+e^-$  pair-electromagnetic pulse of enormous energy that, given an external shock model, could explain the light curves of GRBs. The problem here is that the pair pulse is isotropic, contrary to inferences from observations that GRB ejecta are highly collimated. Moreover, unless the collapse to a black hole takes place well after the SN, it would be difficult for an isotropic explosion to break through the stellar envelope.

Tapping the spin energy of the newly formed black hole seems a better bet for a GRB model. Advocates of a collapsar model generally invoke the Blandford-Znajek process where an induced voltage, formed when the intense accretion-disk magnetic field is shorted out in the ergosphere of the spinning black hole, accelerates particles. For a sufficiently massive and highly magnetized accretion disk surrounding a black hole with spin parameter  $a = Jc/GM^2 \rightarrow 1$ , adequate power can be injected to explain a GRB<sup>9</sup>. Though this is the most popular model for GRBs at the present time, quantitative explanations of temporal and spectral features of GRB-like pulses, the constant energy-upper limit, <sup>56</sup>Ni production, the escape from the stellar envelope of a large  $\Gamma$  outflow, the mean duration of GRB activity, etc. (see Section 5), remain unsolved. Another problem is that simulations of collapse to a

black hole do not leave behind a sufficiently massive torus to power a GRB<sup>5,100</sup>. Such simulations do not give much support for a supranova scenario, either, because differential rotation induces toroidal Alfvén waves that can magnetically brake and destabilize the neutron star, thereby causing collapse within hundreds of seconds.

Another possibility is that the Penrose process, involving either Penrose Compton scattering or Penrose pair production<sup>101,102,103</sup>, extracts energy from the newly formed, rapidly rotating black hole. Particles on retrograde orbits in the ergosphere can extract rotational energy through decay or scattering. It is not clear, however, that retrograde scatterers can be formed in the dynamically forming black-hole, nor is it clear that the efficiencies of this process are adequate to power a GRB.

Given the uncertainties in our knowledge of the fundamental GRB energy release process (“a black hole within a black box”), it might be best to speculate on a viable GRB model from the observations, as summarized earlier.

1. The delayed reddened excesses are indeed due to SNe, and the progenitor star of a GRB collapses to a neutron star to form a Type Ic SNe, forming <sup>56</sup>Ni through explosive nucleosynthesis.
2. The delays between collapses from a neutron star to a black hole last from minutes to days rather than from weeks to months. This means that X-ray features associated with Fe are mistakenly identified, though the signatures of S, Si, and Ca could still be real.
3. During the period between the two collapse events, powerful pulsar winds could evacuate a channel along the rotational axis of the progenitor star and the pulsar, where the overlying material has the smallest column density.
4. A single, highly collimated explosive event during the collapse of the neutron star to a rapidly rotating black hole could eject a relativistic outflow to produce the GRB prompt and afterglow emissions through external shocks with the CBM.

Swift will be crucial to test this and other GRB models by providing better measurements of the X-ray features, by discovering many nearby GRBs from which delayed reddened emissions can be precisely measured, and by searching for signatures of a heated SNR shell.

## Acknowledgments

The work of CD is supported by the Office of Naval Research and *GLAST* Science Investigation Grant No. DPR-S-1563-Y.

## Appendix

### A Pulsar Wind Physics

A pulsar wind (PW) and pulsar wind bubble (PWB) consisting of a quasi-uniform, low density, highly magnetized pair-enriched medium within the SNR shell is formed

by a highly magnetized neutron star during the period of activity preceding its collapse to a black hole<sup>56</sup>. The interaction of the PW with the shell material will fragment and accelerate the SNR shell, and the PW emission will be a source of ambient radiation that can be Comptonized to gamma-ray energies<sup>57,94</sup>.

The nonthermal leptonic PW radiation provides a source of hard ionizing radiation to heat and photoionize material in the SNR shell, which can be described in terms of a partial covering model as a result of the strong PW/SNR interaction. This radiation heats the shell, and the escaping thermalized radiation is seen as the delayed reddened optical excesses in GRB optical afterglow light curves. The source of ionizing nonthermal radiation, which is extinguished when the GRB occurs, would provide a nonthermal precursor to a GRB, though at low flux.

A very rapidly rotating, strongly magnetized neutron star is formed in the first step of the supranova scenario. For a neutron star with surface polar field of  $10^{12}B_{12}$  G, a rotation rate of  $10^4\Omega_4$  rad s<sup>-1</sup>, and a radius of  $15r_{15}$  km, the radiated power  $L_0 \cong 7 \times 10^{44} B_{12}^2 r_{15}^6 \Omega_4^4$  ergs s<sup>-1</sup>. The quantity  $E_{rot} = \frac{1}{2}j(GM^2/c^2)\Omega \cong 2 \times 10^{53} j_{0.5} M_3^2 \Omega_4$  ergs  $\equiv 10^{53} E_{53}^{rot}$  is the initial rotational energy of the neutron star, expressed in terms of the neutron-star mass  $M = 3M_3 M_\odot$  and the dimensionless angular momentum  $j_{0.5} = GM^2/2c$ , which remains roughly constant during collapse<sup>7</sup>. The spin-down time  $t_{sd} = (E_{rot}/L_0) \cong 2.8 \times 10^8 j_{0.5} M_3^2 (B_{12}^2 r_{15}^6 \Omega_4^3)^{-1}$  s.

The torque equation,  $\dot{\Omega} = -K\Omega^n$ , where the braking index  $n = \ddot{\Omega}\Omega/\dot{\Omega}^2$ , can be solved to give  $\Omega(t) = \Omega_0(1 + t/t_d)^{-1/(n-1)}$ , provided that  $K$  remains constant<sup>92</sup>. (For the Crab,  $n = 2.5$ .) We assume that the spin-down power is radiated as a PW in the form of particle and Poynting flux, so that the wind luminosity  $L_w \cong L_{sd} = (\xi_e + \xi_p + \xi_B)L_{sd} = L_0/(1 + t/t_{sd})^k$ , where  $k = (n+1)/(n-1)$ , and we have divided the wind power into leptonic (“e”), hadronic (“p”), and electromagnetic (“B”) fractions  $\xi_i$ ,  $i = e, p, B$ .

In the supranova model, rotational stability is lost due to spindown, and the neutron star collapses to a black hole to produce a GRB at time  $t_{coll}$ . Here we assume  $t_{coll} \lesssim t_{sd}$ , so that for  $k > 1$  the wind energy  $E_w(t) = \eta(k-1)^{-1}L_0 t_{sd} [1 - (1 + (t/t_{sd})^{1-k})^{-k}] \rightarrow \eta L_0 t$  when  $t \lesssim t_{sd}$ , where the parameter  $\eta$  roughly accounts for the escape of wind energy from the SNR shell as well as losses of wind energy due to radiation, and is assumed here to be constant with time. The equation for the SNR shell dynamics in a spherical approximation for the SNR shell is  $M_{SNR}\ddot{R} = 4\pi R^2 p_w(t)$ , where  $M_{SNR} = m_{SNR}M_\odot$  is the SNR shell mass, the wind pressure  $p_w(t) \simeq E_w(t)/3V_{pwb}$ , the PWB volume  $V_{pwb} = 4\pi R^3(t)/3$ , and the PWB radius  $R(t) = \int_0^t dt' v(t')$ . This equation can be solved<sup>94</sup> to give

$$R(t) = v_0 t \left(1 + \sqrt{\frac{t}{t_{acc}}}\right), \text{ where } t_{acc} = \frac{3M_{SNR}v_0^2}{4\eta L_0} \cong 1.9 \times 10^7 \frac{m_{SNR}\beta_{-1}^2}{\eta B_{12}^2 r_{15}^6 \Omega_4^4} \text{ s} \quad (4)$$

It follows that  $t_{acc}/t_{sd} = E_{ke}^{SNR}/\eta E_{rot} \simeq 0.1 E_{52}^{SNR}/\eta E_{53}^{rot}$ , where  $\frac{1}{2}M_{SNR}v_0^2 \cong 9 \times 10^{51} m_{SNR}\beta_{-1}^2 \equiv 10^{52} E_{52}^{SNR}$  ergs is the SNR shell kinetic energy, and  $v_0 = 0.1\beta_{-1}c$  is the SNR shell coasting speed. If  $\eta \cong 1$ , then  $t_{acc} \ll t_{sd}$  for standard values, and shell acceleration must be considered. A highly porous shell has  $\eta \ll 1$ . This will occur for strong clumping of the ejecta, which takes place on the Rayleigh-Taylor timescale<sup>57</sup>  $t_{RT} \simeq \sqrt{x/\ddot{R}}$ , where the characteristic clumping size scale is



$x \equiv fR$ . Hence  $(t_{RT}/t_{acc}) = f^{1/2} (t/t_{acc})^{3/4}$  in the regime  $t \lesssim t_{acc}$ . This shows that small-scale ( $f \ll R$ ) clumping will occur when  $f \ll \sqrt{t/t_{acc}}$ . Only a detailed hydrodynamic simulation can characterize the porosity of the shell due to effects of the pulsar wind, which  $\eta$  parameterizes. Here we assume, in contrast to the picture of Ref. [56], that a large fraction of the wind energy escapes the SNR shell and  $\eta \sim 0.1$ , so that shell acceleration can be neglected. This effect also causes the shell to become effectively Thomson thin much earlier than estimated on the basis of a uniform shell approximation, except for high density clouds with small covering factor. A general treatment is needed to treat shell dynamics, including travel-time delays of the pulsar wind and deceleration of the SNR shell by the surrounding medium. When  $t_{coll} \lesssim t_{acc}, t_{sd}$ , as assumed here,  $R \cong v_0 t$ .

The strong PW provides a source of nonthermal leptons, hadrons, and electromagnetic field. Dominant radiation components considered here are leptonic synchrotron and SSC radiation, and thermal emission from the inner surface of the SNR shell which is heated by the nonthermal radiation.

#### A.1 Wind Synchrotron Radiation

The volume-averaged mean magnetic field  $B_w$  in the SNR cavity powered by the PW is obtained by relating the wind magnetic field energy density  $u_B = B_w^2(t)/8\pi = e_{Bw} u_w(t) = 3e_{Bw}\eta L_0 t/4\pi R^3$  through the magnetic-field parameter  $e_{Bw}$ , also assumed to be constant in time. Thus

$$B_w(t) = \frac{\mathcal{B}}{t}, \text{ where } \mathcal{B} = \sqrt{\frac{6e_{Bw}L_0\eta}{v_0^3}} \cong 4 \times 10^8 \sqrt{e_{Bw}\eta} \left( \frac{B_{12}r_{15}^3\Omega_4^2}{\beta_{-1}^{3/2}} \right) \text{ G-s}. \quad (5)$$

Let  $\gamma_w = 10^5\gamma_5$  represent the typical Lorentz factors of leptons in the wind zone of the pulsar. This value should remain roughly constant when  $t \lesssim t_{sd}$ . A quasi-monoenergetic proton/ion wind may also be formed, though we only consider leptonic processes here, and furthermore do not treat nonthermal particle acceleration at the PW/SNR shell boundary shock. When synchrotron losses dominate, the mean Lorentz factor of a distribution of leptons with random pitch angles evolves in response to a randomly oriented magnetic field of mean strength  $B$  according to the expression  $-\dot{\gamma}_{syn} = (\sigma_T B^2/6\pi m_e c)\gamma^2$ , giving

$$\gamma_w = \left[ \frac{1}{\gamma} - T_B \left( \frac{1}{t_i} - \frac{1}{t} \right) \right]^{-1}, \quad (6)$$

where  $t_i$  is the injection time,  $\gamma_i = \gamma_w$  is the injection Lorentz factor, and

$$T_B \gamma_w = \frac{\sigma_T \mathcal{B}^2}{6\pi m_e c} \gamma_w \simeq 2 \times 10^{13} e_{Bw}\eta \left( \frac{B_{12}^2 r_{15}^6 \Omega_4^4}{\beta_{-1}^3} \right) \gamma_5 \text{ s}. \quad (7)$$

Writing the nonthermal electron injection function as

$$\frac{dN_e(\gamma_i, t_i)}{dt_i d\gamma_i} = \frac{\eta \zeta_e L_0}{m_e c^2 \gamma_w} \delta(\gamma_i - \gamma_w), \quad (8)$$

the electron Lorentz factor distribution  $dN_e(\gamma; t)/d\gamma$  can be solved to give

$$\gamma^2 \frac{dN_e(\gamma; t)}{d\gamma} = \dot{N}_e T_B \gamma_w^2 \left( \frac{1}{t} + \frac{1}{\tilde{\gamma}} - 1 \right)^{-2}. \quad (9)$$

In this expression,  $\dot{N}_e \equiv \eta \xi_e L_0 / (m_e c^2 \gamma_w)$ , and we introduce the dimensionless quantities  $\hat{t} = t / T_B \gamma_w$  and  $\hat{\gamma} = \gamma / \gamma_w$ . Adiabatic losses, which are significant on time scales  $\sim t/3$ , are negligible in comparison with synchrotron losses of wind electrons when  $\hat{t} \ll 1$ , and we restrict ourselves to this regime.

The  $\nu L_\nu$  synchrotron radiation flux  $\nu L_\nu^{syn} \simeq \frac{1}{2} u_B c \sigma_T \gamma_s^3 N_e(\gamma_s)$ , where  $\gamma_s = \sqrt{\epsilon/\epsilon_B}$ ,  $\epsilon = h\nu/m_e c^2$ ,  $\epsilon_B = B/B_{cr}$ , and the critical magnetic field  $B_{cr} = 4.41 \times 10^{13}$  G. Thus

$$\nu L_\nu^{syn}(\epsilon) = c \sigma_T \frac{B_{cr}^2}{16\pi} (\dot{N}_e T_B \gamma_w^2) \left(\frac{u}{\hat{t}}\right)^{3/2} \sqrt{\epsilon} \left(\frac{1}{\hat{t}} + \sqrt{\frac{u \gamma_w^2}{\epsilon \hat{t}} - 1}\right)^{-2}, \quad \text{for } \epsilon \leq \epsilon_{max}, \quad (10)$$

where  $u \equiv \mathcal{B}/\gamma_w B_{cr} T_B \simeq 4.5 \times 10^{-19} \beta_{-1}^3 / (\sqrt{\eta e_{Bw}} B_{12} r_{15}^3 \Omega_4^2 \gamma_5)$ , and

$$\epsilon_{max} \simeq \epsilon_B \gamma_w^2 = \frac{\mathcal{B}}{B_{cr}} \frac{\gamma_w^2}{t} \simeq \frac{4.4 \times 10^{-9}}{\hat{t}} \frac{\beta_{-1}^{3/2} \gamma_5}{\sqrt{\eta e_{Bw}} B_{12} r_{15}^3 \Omega_4^2}. \quad (11)$$

The synchrotron cooling timescale for wind electrons is  $t_{syn} = \gamma_w T_B \hat{t}^2$ . In the regime  $\hat{t} \lesssim \beta_0$  where the wind electrons strongly cool, we can approximate the synchrotron spectrum by

$$\nu L_\nu^{syn}(\epsilon) \simeq \frac{3}{8} \xi_e L_0 \left(\frac{\epsilon}{\epsilon_{max}}\right)^{1/2} H(\epsilon; \epsilon_0, \epsilon_{max}), \quad (12)$$

where  $H(x; a, b) = 1$  for  $a \leq x < b$ , and  $H = 0$  otherwise. The value of  $\hat{t}$  at  $t_{sd}$  is

$$\frac{t_{sd}}{T_B \gamma_w} \simeq 1.4 \times 10^{-5} \frac{j_{0.5} M_3^2 \beta_{-1}^3}{e_{Bw} \eta B_{12}^6 r_{15}^{18} \Omega_4^{11} \gamma_5}. \quad (13)$$

Strong cooling holds when  $\hat{t} < t_{sd}/T_B \gamma_w$ , noting that time in physical units can be found from equation (7).

## A.2 Wind Synchrotron Self-Compton Radiation

The relative importance of synchrotron self-Compton (SSC) to synchrotron cooling is given by the ratio  $\rho = u_{syn}/u_B$  of the synchrotron radiation energy density to  $u_B = \mathcal{B}^2/8\pi t^2$  (see eq.[5]). The PW synchrotron radiation energy density  $u_{syn} \simeq \kappa(\nu L_\nu^{max})/4\pi R^2 c$ , where  $\nu L_\nu^{max} \simeq \xi_e L_0$  and the parameter  $\kappa \geq 1$  is a reflection factor such that  $\kappa = 1$  corresponds to perfect absorption or direct escape (small covering factor) of the PW synchrotron radiation, and  $\kappa \gg 1$  corresponds to a highly reflecting SNR shell with large covering factor. One obtains  $\rho = 0.033 \kappa \xi_e \beta_{-1} / e_{Bw} \eta$ . For large porosity with  $\kappa \simeq 1$  and  $\eta \approx 0.1$ , we see that the SSC contribution is small compared to the synchrotron flux when  $\xi_e \beta_{-1} / e_{Bw} \lesssim 1$ . We restrict ourselves to this regime where equation (6) is valid.

In the  $\delta$ -function approximation for the energy gained by a photon upon being scattered by relativistic electrons<sup>104</sup>, with scattering restricted to the Thomson regime, the  $\nu L_\nu$  SSC spectrum from the cooling wind electrons is given by

$$\nu L_\nu^{SSC} \simeq \frac{\sigma_T \kappa \xi_e L_0}{8\pi v_0^2 T_B} \frac{\dot{N}_e}{\hat{t}^2} \sqrt{\frac{\epsilon}{\epsilon_{max}}} \left[ \frac{1}{a_0(a_0 + x)} + a_0^{-2} \ln\left(\frac{x}{a_0 + x}\right) \right] \Big|_{x_0}^{x_1}, \quad (14)$$

where  $a_0 = \hat{t}^{-1} - 1$ ,  $x_0 = \gamma_w \sqrt{\epsilon_0/\epsilon}$ , and  $x_1 = \gamma_w \sqrt{\max(\epsilon, \epsilon^{-1}, \epsilon_{max})/\epsilon}$ , where we have used approximation (12) for the synchrotron spectrum.

### A.3 Thermal Emission from the Interior of the Shell

The SNR shell is pictured as having been shredded by the PW and therefore highly porous, though permeated with small scale ( $\sim 10^{12}$ - $10^{14}$  cm) density irregularities consisting largely of metals<sup>17,50</sup>. Note that  $0.1m_{56,-1}M_\odot$  of  $^{56}\text{Ni}$  provides a radioactive decay power of  $\sim 2 \times 10^{42}m_{56,-1}$  ergs  $\text{s}^{-1}$  before decaying on an  $\approx 120$  day timescale. The partial covering factor  $p_c$  ( $\leq 1$ ) corresponds to the covering fraction by optically-thick, dense shell inhomogeneities. Recognizing the severe limitations in the following expression, we determine the effective temperature  $T_{eff}$  in the interior of the shell through the relation

$$4\pi R^2 \sigma_{\text{SB}} T_{eff}^4 p_c \cong \mathcal{A} p_c \frac{\xi_e L_0}{\kappa} + 2 \times 10^{42} m_{56,-1} \exp(-t/120 \text{ d}) \text{ ergs s}^{-1}, \quad (15)$$

where  $\mathcal{A}(\leq 1)$  is an absorption coefficient, dependent in general on the evolving radiation spectrum, though  $\mathcal{A}$  is here assumed constant. The wind heating is more important than heating from the decay of radioactive Ni when  $(\mathcal{A}/0.1)(p_c/0.1)(\xi_e/1/3) \gtrsim m_{56,-1}/B_{12}^2 r_{15}^6 \Omega_4^4$ . In this regime,

$$T_{eff} = \left( \frac{\mathcal{A} \xi_e L_0}{4\pi R^2 \sigma_{\text{SB}}} \right)^{1/4} \approx \frac{825 \mathcal{A}^{1/4}}{\sqrt{t/t_{sd}}} \left( \frac{\xi_e}{1/3} \right)^{1/4} \frac{B_{12}^{3/2} r_{15}^{9/2} \Omega_4^{5/3}}{\sqrt{j_{0.5} \beta_{-1} M_3}} \text{ K}, \quad (16)$$

letting  $\kappa \approx 1$  because  $p_c \sim 0.1$ . For standard parameters, the shell is heated to  $\sim 10^4$  K temperatures when  $t/t_{sd} \ll 1$ . When  $B_{12} \gtrsim 4$ , this occurs at  $t/t_{sd} \lesssim 1$ . The PW heat source is extinguished once the GRB occurs, and the thermal emission from the SNR shell will decay on the dynamical timescale  $t_{dyn} = R(t)/c \cong 324 \beta_{-1} (j_{0.5} M_e^2 / B_{12}^2 r_{15}^6 \Omega_4^3) (t/t_{sd})$  d, noting that the cooling timescale of a hot shell is generally shorter than  $t_{dyn}$ .

The parameters used in Fig. 1 are  $j_{0.5} = B_{12} = r_{15} = \Omega_4 = \beta_{-1} = \kappa = M_3 = m_{52,-1} = \gamma_5 = 1$ ,  $\xi_e = e_{Bw} = 1/3$ , and  $p_c = \eta = \mathcal{A} = 0.1$ .

## References

1. M. Böttcher, in the Tenth Marcel Grossmann Meeting on General Relativity, Rio de Janeiro, Brazil (July 20-26, 2003), astro-ph/0312538 (2004).
2. D. Lazzati, in the Tenth Marcel Grossmann Meeting on General Relativity, Rio de Janeiro, Brazil (July 20-26, 2003), astro-ph/0402058 (2004).
3. J. Hjorth et al., Nature 423 (2003) 847.
4. J. Pruet, R. Surman, and G. C. McLaughlin, ApJ, 602 (2004) L101.
5. S. L. Shapiro (2004) astro-ph/0404338.
6. K. S. Wood, P. F. Michelson, and C. D. Dermer, in preparation (2004).
7. M. Vietri and L. Stella, Astrophys. J., 507 (1998) L45.
8. P. A. Price, et al., ApJ, 571 (2002) L121.
9. A. I. MacFadyen, S. E. Woosley, and A. Heger, ApJ, 550 (2001) 410
10. A. Burrows, private communication (2004).

11. S. E. Woosley, *Astrophys. J.* 405 (1993) 273.
12. M. Vietri and L. Stella, *Astrophys. J.* 527 (1999) L43.
13. S. Kulkarni, website (<http://www.astro.caltech.edu/~srk/>) presentations (2004).
14. D. A. Frail et al., *Astrophys. J.* 562 (2001) L55.
15. J. S. Bloom, D. A. Frail, and S. R. Kulkarni, *S. R.*, *ApJ*, 594 (2003) 674.
16. A. Panaitescu and P. Kumar, *Astrophys. J.* 554 (2001) 667.
17. C. D. Dermer and K. E. Mitman, *ApJ*, 513 (1999) L5.
18. C. D. Dermer and K. E. Mitman, in “Gamma Ray Bursts in the afterglow era - Third Rome Workshop,” (2003) (astro-ph/0301340).
19. V. V. Usov, *Nature*, 357, (1992) 472.
20. J. van Paradijs, C. Kouveliotou, and R. A. M. J. Wijers, *Ann. Rev. Astron. Astrophys.* 38 (2000) 379.
21. B. Zhang and P. Mészáros, *Intern. J. Modern Physics A*, in press, astro-ph/0311321 (2003).
22. C. D. Dermer, in Proc. 27th ICRC, Hamburg, Germany (7-15 August 2001), (2002) astro-ph/0202254
23. T. Piran, *Phys. Reports* 314 (1999) 575.
24. P. Mészáros, 2002, *ARAA*, 40, (2002) 137.
25. Y. Lithwick and R. Sari, 555 (2001) 540 .
26. C. D. Dermer, in the Tenth Marcel Grossman Meeting on General Relativity, Rio de Janeiro, Brazil (2004), astro-ph/0402438.
27. S. Razzaque, P. Mészáros, and B. Zhang, *ApJ*, submitted (2004) (astro-ph/0404076).
28. S. G. Djorgovski et al., in *Gamma Ray Bursts in the Afterglow Era*, E. Costa et al., eds. (Springer: Berlin, 2001), 218.
29. J. S. Bloom, Ph.D. thesis, CalTech (2002).
30. J. S. Bloom et al., *Astrophys. J.* 518 (1999) L1.
31. T. J. Galama, R. A. M. J. Wijers, *Astrophys. J.* 549 (2001) L209.
32. D. Q. Lamb, et al., *New Astronomy Review*, 48 (2004) 423.
33. K. Z. Stanek, P. M. Garnavich, J. Kaluzny, W. Pych, and I. Thompson, *I.*, *ApJ*, 522 (1999) L39.
34. C. D. Dermer, *ApJ*, 574 (2002) 65.
35. L. Piro, et al. *Astrophys. J.* 514 (1999) L73.
36. A. Yoshida et al., *Astrophys. J.* 557 (2001) L27.
37. L. Piro, et al. *Science* 290 (2000) 955.
38. L. Amati, et al. *Science* 290 (2000) 953.
39. L. A. Antonelli et al., *Astrophys. J.* 545 (2000) L39.
40. J. N. Reeves et al., *Nature* 416 (2002) 512.
41. N. R. Butler et al., *ApJ*, 597 (2003) 1010.
42. D. Watson et al., *A&A*, 393 (2002) L1.
43. G. C. McLaughlin et al. *ApJ*, 567 (2002) 454.
44. G. C. McLaughlin and R. Wijers, *ApJ*, 580 (2002) 1017.
45. M. Vietri, C. Perola, L. Piro, and L. Stella, *MNRAS* 308 (1999) L29.
46. D. Lazzati, G. Ghisellini, L. Amati, F. Frontera, M. Vietri, L. Stella, *Astrophys. J.* 556 (2001) 471.

47. M. Böttcher, 539 (2000) 102.
48. M. Böttcher and C. L. Fryer, 547 (2001) 338.
49. M. Böttcher, C. D. Dermer, A. W. Crider, E. P. Liang, A&A 343 (1999) 111.
50. M. Böttcher, C. L. Fryer, C. D. Dermer, Astrophys. J. 567 (2002) 441.
51. D. Lazzati, E. Ramirez-Ruiz, and M. J. Rees, ApJ, 572 (2002) L57.
52. M. J. Rees, and P. Mészáros, ApJ, 545 (2000) L73.
53. F. Tavecchio, G. Ghisellini, and D. Lazzati, A&A, 415 (2004) 443.
54. P. Kumar and R. Narayan, ApJ, 584 (2003) 895.
55. C. L. Fryer, S. E. Woosley, D. Hartmann, Astrophys. J. 526 (1999) 152.
56. A. Königl, and J. Granot, Astrophys. J., 574 (2002) 134.
57. Inoue, S., Guetta, D., and Pacini, F. 2003, Astrophys. J. 583 (2003) 379.
58. D. L. Freedman and E. Waxman, ApJ, 547 (2001) 922.
59. S. Kulkarni et al., Nature, 395 (1998) 663.
60. K. Iwamoto et al., Nature, 395 (1998) 672.
61. R. Willingale, et al., MNRAS, 349 (2004) 31.
62. Soderberg, A. Ph.D. thesis, CalTech, in preparation (2004).
63. J. N. Bahcall, et al., ApJ, 452 (1995) L91.
64. D. E. Reichart, Astrophys. J. 521 (1999) L111.
65. T. J. Galama, et al., ApJ, 536 (2000) 185.
66. J. S. Bloom, et al., Nature, 401 (1999a) 453.
67. T. Galama et al., Nature, 397 (1998) 670.
68. E. Pian et al., Astrophys. J. 536 (2000) 778.
69. S. Holland et al., A&A, 371 (2001) 52.
70. E. Berger et al. ApJ, 556 (2001) 556.
71. Lazzati, D., et al. 2001a, A&A, 378, 996
72. J. S. Bloom, et al. Astrophys. J. 572 (2002) L45.
73. P. A. Price, et al., ApJ, 584 (2003) 931.
74. P. A. Price, et al., ApJ, 589 (2003a) 838.
75. E. Berger, A. M. Soderberg, D. A. Frail, and S. R. Kulkarni, ApJ, 587 (2003) L5.
76. A. Levan, et al., ApJ, submitted (2004) (astro-ph/0403450).
77. L. Nicastro, et al., A&A, submitted (2004) (astro-ph/0403584).
78. K. Z. Stanek et al., ApJ, 591 (2003) L17.
79. Y. M. Lipkin, et al., ApJ, 606 (2004) 381.
80. B. Thomsen, et al., A&A, submitted (2004) (astro-ph/0403451).
81. C. D. Matzner, MNRAS, 345 (2003) 575.
82. L. Amati, et al., A&A, 390 (2002) 81.
83. D. Lazzati, E. Rossi, S. Covino, G. Ghisellini, and D. Malesani, A&A, 396 (2002) L5.
84. X. Wang and A. Loeb, ApJ, 535 (2000) 788
85. L. Borgonovo and F. Ryde, ApJ, 548 (2001) 770.
86. C. D. Dermer, ApJ, submitted (2004a) (astro-ph/0403508).
87. C. D. Dermer, M. Böttcher, and J. Chiang, Astrophys. J. 515 (1999) L49.
88. M. Böttcher and C. D. Dermer, Astrophys. J. 529 (2000) 635, (e) 536 (2000) 513.
89. C. D. Dermer, preprint (2002) (astro-ph/0211300).

90. Wang, W., & Woosley, S. E.. 2002, Proc. of 3D Stellar Evolution Workshop, Livermore, CA (July 2002) (astro-ph/0209482)
91. D. R. Ballantyne, E. Ramirez-Ruiz, D. Lazzati, D., and L. Piro, A&A, 389 (2002) L74.
92. A. M. Atoyan, A&A, 346 (1999) L49.
93. D. Lazzati, S. Campana, S., and G. Ghisellini, MNRAS, 304 (1999) L31.
94. D. Guetta, D. and J. Granot, MNRAS340 (2003), 340, 115.
95. C. D. Dermer and A. M. Atoyan, PRL, 91 (2003) 071102.
96. D. Guetta, D. and J. Granot, PRL, 90 (2003) 201103.
97. S. Razzaque, P. Mészáros, P., and E. Waxman, PRL 90 (2004) 241103
98. G. Lugones, J. E. Horvath, E. M. de Gouveia dal Pino, and C. R. Ghezzi, in the Tenth Marcel Grossmann Meeting on General Relativity, Rio de Janeiro, Brazil (July 20-26, 2003), (2004).
99. C. L. Bianco, R. Ruffini, and S.-S. Xue, A&A, 368, (2001) 377.
100. S. L. Shapiro, ApJ, 544 (2000) 397.
101. T. Piran and J. Shaham, PRD, 16 (1977) 1615.
102. D. Leiter and M. Kafatos, ApJ, 226 (1978) 32.
103. R. K. Williams, PRD, 51 (1995) 5387.
104. C. D. Dermer, S. J. Sturmer, and R. Schlickeiser, ApJS, 109 (1997) 103.